1 December 2012 Volume 112 Number 11

AIP Journal of Applied Physics

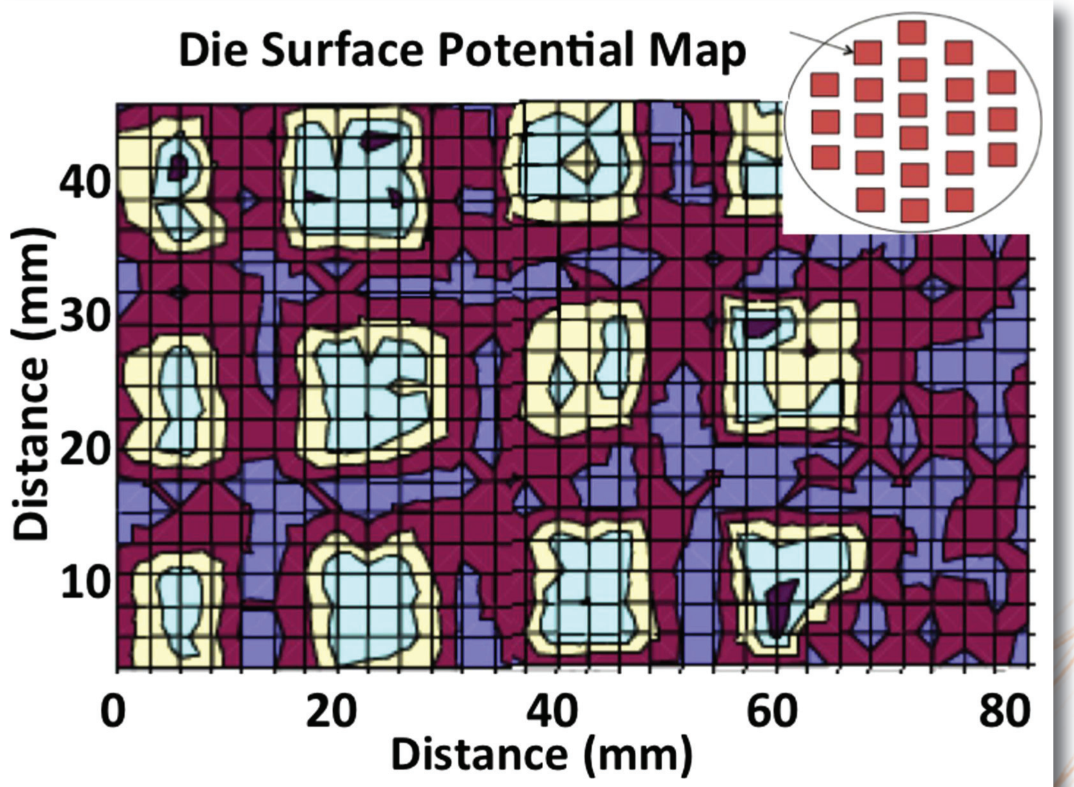

APPLIED PHYSICS REVIEWS:

The effects of vacuum ultraviolet radiation on low-*k* dielectric films

by H. Sinha, H. Ren, M. T. Nichols, J. L. Lauer,
M. Tomoyasu, N. M. Russell, G. Jiang, G. A. Antonelli,
N. C. Fuller, S. U. Engelmann, Q. Lin, V. Ryan,
Y. Nishi, and J. L. Shohet

jap.aip.org

AIP | Journal of Applied Physics

The effects of vacuum ultraviolet radiation on low-k dielectric films

H. Sinha, H. Ren, M. T. Nichols, J. L. Lauer, M. Tomoyasu et al.

Citation: J. Appl. Phys. **112**, 111101 (2012); doi: 10.1063/1.4751317

View online: http://dx.doi.org/10.1063/1.4751317

View Table of Contents: http://jap.aip.org/resource/1/JAPIAU/v112/i11

Published by the American Institute of Physics.

JOURNAL OF APPLIED PHYSICS **112**, 111101 (2012)

APPLIED PHYSICS REVIEWS—FOCUSED REVIEW

The effects of vacuum ultraviolet radiation on low-*k* dielectric films

H. Sinha,[1] H. Ren,[1] M. T. Nichols,[1] J. L. Lauer,[1] M. Tomoyasu,[2] N. M. Russell,[2] G. Jiang,[3] G. A. Antonelli,[3] N. C. Fuller,[4] S. U. Engelmann,[4] Q. Lin,[4] V. Ryan,[5] Y. Nishi,[6] and J. L. Shohet[1]
[1] *University of Wisconsin-Madison, Madison, Wisconsin 53706, USA*
[2] *Tokyo Electron Limited, Albany, New York 12203, USA*
[3] *Novellus Systems, Tualatin, Oregon 97062, USA*
[4] *IBM Watson Research Center, Yorktown Heights, New York 10598, USA*
[5] *GLOBALFOUNDRIES, Albany, New York 12203, USA*
[6] *Stanford University, Stanford, California 94305, USA*

(Received 2 September 2011; accepted 13 August 2012; published online 4 December 2012)

Plasmas, known to emit high levels of vacuum ultraviolet (VUV) radiation, are used in the semiconductor industry for processing of low-*k* organosilicate glass (SiCOH) dielectric device structures. VUV irradiation induces photoconduction, photoemission, and photoinjection. These effects generate trapped charges within the dielectric film, which can degrade electrical properties of the dielectric. The amount of charge accumulation in low-*k* dielectrics depends on factors that affect photoconduction, photoemission, and photoinjection. Changes in the photo and intrinsic conductivities of SiCOH are also ascribed to the changes in the numbers of charged traps generated during VUV irradiation. The dielectric-substrate interface controls charge trapping by affecting photoinjection of charged carriers into the dielectric from the substrate. The number of trapped charges increases with increasing porosity of SiCOH because of charge trapping sites in the nanopores. Modifications to these three parameters, i.e., (1) VUV induced charge generation, (2) dielectric-substrate interface, and (3) porosity of dielectrics, can be used to reduce trapped-charge accumulation during processing of low-κ SiCOH dielectrics. Photons from the plasma are responsible for trapped-charge accumulation within the dielectric, while ions stick primarily to the surface of the dielectrics. In addition, as the dielectric constant was decreased by adding porosity, the defect concentrations increased.
[http://dx.doi.org/10.1063/1.4751317]

TABLE OF CONTENTS

I. INTRODUCTION AND BACKGROUND 1
II. CHARGE TRAPPING 2
III. EXPOSURE SYSTEMS 3
  A. Synchrotron radiation 3
  B. Electron cyclotron resonance (ECR) plasma 3
IV. MEASUREMENT TECHNIQUES 4
  A. Substrate/photoemission currents.......... 4
  B. VUV spectroscopy 4
  C. Surface-potential measurements........... 5
  D. Capacitance-voltage characteristics........ 5
  E. Electron-spin resonance (ESR) spectroscopy 5
V. DIELECTRIC MATERIALS 6
VI. SYNCHROTRON EXPOSURE 7
  A. VUV spectroscopy...................... 7
  B. CV and surface potential measurements ... 7
  C. Effect of ultraviolet (UV) curing on charge trapping 7
  D. Effect of dielectric-substrate interface on charge trapping......................... 9
  E. Effect of porosity on charge trapping 11
VII. PLASMA EXPOSURE...................... 12
  A. Charge accumulation in low-k dielectrics . 12
  B. Modifications of chemical bonds and physical changes 13
VIII. SUMMARY AND CONCLUSIONS 14

I. INTRODUCTION AND BACKGROUND

Porous low-*k* organosilicate dielectrics are replacing SiO_2 as the preferred inter-metal dielectric film to reduce signal propagation delay and power dissipation in ULSI circuits.[1,2] A critical challenge in plasma processing of these porous materials is their sensitivity to charging, chemical and physical damage, and time-dependent dielectric breakdown (TDDB) failure as a result of plasma exposure.[3–7] During plasma processing, ion bombardment, vacuum ultraviolet (VUV) irradiation, and free-radical flux can occur.[8–11] These are of concern because the critical dimensions are now the same size as the penetration depth of particles and photons.

VUV radiation has been found to introduce photoconductive effects[12,13] which govern the density and location of trapped charges within the dielectric.[14–17] In addition, trapped charges generated by VUV irradiation of low-*k* dielectrics have been shown to adversely affect the capacitance,[18] breakdown voltage,[19] and leakage currents[20,21] without any chemical or structural change in SiCOH. This review demonstrates how VUV irradiation causes generation of trapped charges in SiCOH and how it can be reduced. In describing ways to reduce trapped charges, we also describe methods to determine the number of trapped charges in the dielectric.[22] Furthermore, the effect of VUV irradiation on charge trapping, chemical changes, and changes in defect state concentration are contrasted with that of ion bombardment during plasma exposure.

Using synchrotron VUV radiation, particle bombardment can be eliminated from photon bombardment.[23] During plasma exposure, differentiation between the effects of charged particle bombardment and VUV irradiation during plasma exposure can be achieved by using a capillary-array window[24] that effectively shields the dielectric from charged-particle bombardment without disrupting VUV irradiation. After simultaneous plasma exposure to both uncovered and array-covered dielectrics, the changes caused by VUV irradiation and ion bombardment to the electrical, chemical, and physical properties of the dielectric can be examined.

Studies of low-*k* porous SiCOH have concentrated on determining the defect-state density and their effects on dielectric functionality and reliability. High defect-state density often leads to significant charge trapping in porous low-k SiCOH which, in turn, has a detrimental effect on its reliability.[25] Guedj *et al.* have shown through x-ray photoemission spectroscopy that the binding energy of atoms in SiCOH decreases with charge trapping.[6] They also deduced that irreversible degradation of the dielectric could occur. Although their study used thermal stress as the energy source, VUV irradiation can have a similar effect since both techniques cause generation of trapped charge.

A known technique to reduce radiation damage is to optimize the plasma gas chemistry.[26] Ishikawa *et al.*[27] have shown on SiO_2 and Si_3N_4 that, through plasma gas optimization, radiation-induced damage could be reduced. However, the defect-state density in SiCOH is higher than in SiO_2 or Si_3N_4. It has been reported by Atkin *et al.*[15] from impedance measurements that low-*k* porous SiCOH has a significantly higher density of defect states as compared to silicon dioxide. Hence plasma-gas optimization was not sufficient. In addition, SiCOH has mechanisms of charge trapping beyond those in SiO_2 and Si_3N_4. First, it has been reported by Chao *et al.*[28] that the SiCOH surface has increased dangling bonds, as compared to SiO_2, where charge trapping can occur. Second, through a theoretical approach, Planelles *et al.*[29] showed that charges can be trapped in pores of SiCOH. Thus more investigation is required to understand the mechanisms behind the generation of trapped charge in SiCOH and to develop ways to reduce it.

II. CHARGE TRAPPING

VUV irradiation of dielectrics can cause electron-hole pair generation, photoconduction, photoemission, and photoinjection of electrons from the substrate into the dielectric.[30–34] These processes depend on the incident photon energy and the dielectric composition and thickness. Electron-hole pairs will be formed if electrons are excited into the conduction band from the valence band or from defect states within the dielectric.[34] The behavior of photoconduction, photoemitted, and photoinjected electrons will then depend on the energy of the generated electron. That is, depending on their energy, the electrons and holes can travel in the dielectric, i.e., photoconduction or remain trapped at a fixed location. It is expected that electrons will dominate photoconduction, photoemission, and photoinjection, because the mobility of electrons is much larger than the mobility of holes.[35]

When the energy supplied by irradiation is greater than the sum of the bandgap energy and the electron affinity (i.e., photoemission threshold), photoemission can occur from the valence band of the dielectric and/or the defect states in the bulk of the dielectric.[28] An electron with energy lower than the photoemission threshold could gain additional energy from another process and be photoemitted. Thus, photoemission from the defect states leads to depopulation of electrons from the dielectric. Therefore, after photoemission, a dielectric develops a net positive charge.

Photons with energies greater than the bandgap energy but lower than the photoemission threshold, will create electron-hole pairs, which remain within the dielectric layer. The electrons and holes may separate due to their initial energies and/or the presence of an electric field within the dielectric layer resulting in a photoconduction current.

In addition to VUV photons being absorbed in the dielectric, they can also be absorbed in the substrate. For this to occur, the photons must penetrate through the dielectric. Photoabsorption in the substrate can thus result in electron-hole pairs begin created in the substrate. Similarly to the dielectric, electrons in the substrate can photoconduct. In addition, these electrons can be photoinjected into the dielectric. For photoinjection to occur, the substrate-dielectric interface-energy barrier should be less than the energy of the electrons. For example, the Si-SiCOH interface has an energy barrier of 4 ± 0.5 eV.[15,18,20] As a result, only electrons in silicon with energies greater than 4.5 eV can be injected into SiCOH from Si. A reverse process whereby electrons are injected from the dielectric into the substrate can also occur. But the probability of an electron being injected from the substrate into the dielectric is higher since the electrons generated in the substrate tend to have a higher energy than the ones in the dielectric because the band gap of Si is smaller than that for SiCOH. Photoinjection can be further enhanced by the presence of trapped charges in SiCOH at the interface that reduces the interface energy barrier by acting as a low-energy conduction pathway.[36]

It is plausible that photoinjected electrons generate a drift/diffusion current from the substrate-dielectric interface to the dielectric-vacuum interface, where electrons can be photoemitted.[37,38] Thus, at any given time during VUV irradiation, photoemitted electrons are the result of (1) depopulated electrons from the defect states and (2) photoinjected electrons. Trapped charges from the depopulation of defect states will continue to be created until a steady state is achieved. At this point, no more net trapped charge will be generated in the dielectric, and the photoemitted electron flux will then be equal to the flux of the photoinjected electrons. In order to have a complete circuit, charge conservation dictates that when the substrate is connected to ground, the photoemitted electrons are returned to the substrate. Thus, under these conditions in steady state, the photoemission current is equal to the substrate current.

To illustrate, suppose an electron is photoemitted. The vacuum chamber collects the photoemitted electrons. If both the chamber and the substrate are grounded in the system, the electrons flow back into the substrate. Since VUV irradiation is still occurring, this enables the electrons to be photoinjected back into the dielectric. Once the electrons are in the dielectric, they can undergo drift/diffusion followed by photoemission, and the cycle continues.

As the trapped charge increases in the dielectric, a self-consistent electric field appears.[38] The self-consistent electric field acts as a barrier for electrons leaving the dielectric and hence reduces photoemission. This continues until steady state. In steady state, no additional trapped charges are generated, and hence the electric field attains its maximum and steady state value. The self-consistent electric fields have been estimated to be in order of MV/m in dielectrics.[38] Although numerical simulation of electron motion has not been done for porous SiCOH, calculations for SiN have showed that the self-consistent electric field indeed acts a barrier to the number of trapped charges being generated in the dielectric.[39]

Thus, each of the three primary processes (photoemission, photoinjection, and photoconduction) competes with the others to influence charge accumulation during VUV irradiation.[40] Photoemission of electrons from defect states *depopulates* these states of electrons, resulting in accumulation of net positive charge. Conversely, photoinjection can *repopulate* vacant defect states in the dielectric with electrons from the substrate, resulting in a net depletion of trapped positive charge.[36,38,39,47,48]

III. EXPOSURE SYSTEMS

A. Synchrotron radiation

Most dielectrics have an energy bandgap that lies between 5 and 10 eV, which is within the vacuum ultraviolet range (10–200 nm, 6.2–124 eV).[41] As a result, VUV photons produce photoemissive, photoconductive, and photoinjective processes within dielectrics. Thus, an obvious choice to examine the VUV response of dielectric films as a function of VUV photon energy is synchrotron radiation. The synchrotron exposure system used here is shown in Figure 1. It consists of a dielectric-coated wafer with a 100 × 100 mm square aluminum plate placed 3.5 cm in front of the wafer. In the center of the Al plate there is a rectangular opening 20 × 50 mm in size to allow the VUV photons to be normally incident on the surface of the wafer. The aluminum plate can collect photoemitted electrons, which allows for the simultaneous measurement of the photoemission current and the current drawn by the substrate during VUV exposure. This system was inserted in a vacuum chamber at a distance of 5 feet from the exit slit of a normal-incidence Seya-Namioka VUV monochromator at the University of Wisconsin Synchrotron Radiation Center (SRC). The monochromator has an output-energy range between 4 and 30 eV and a bandpass of 0.3 nm. During VUV irradiation, the vacuum chamber was evacuated to a pressure of 10^{-8} Torr. At the location of the wafer, the photon beam is elliptical and measured to be roughly 25 mm × 10 mm on the wafer surface. As shown in Figure 1, the substrate is grounded during VUV irradiation, while a dc-bias voltage of +48 V is placed on the Al plate to ensure that the Al plate collects most of the photoemitted electrons. The photoemission current and the current drawn by the substrate are each measured with a Keithley 486 picoammeter.

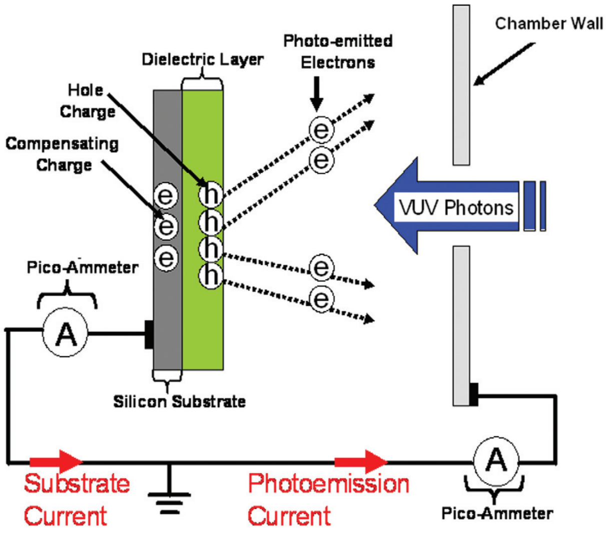

FIG. 1. Experimental set-up for synchrotron irradiation of dielectric films and to measure substrate/photoemission current.

With the arrangement shown in Figure 1, two types of experiments are performed to characterize (1) the accumulation of charge within dielectrics during VUV irradiation and (2) the valence-band structure and energy levels of trap states within the bandgap of dielectrics using VUV spectroscopy. In both cases, the currents drawn by the Al plate and the substrate during VUV irradiation are measured. However, in case (1), a single photon energy is used, while in case (2) the photon energy is rapidly scanned over a range of energies, for example, between 5 and 15 eV. However, during this VUV spectroscopy, special care must be taken to ensure that the photon flux is small enough so that modification of the dielectric is minimized emphasizing the need for a rapid scan. In these experiments, the photon flux is approximately two orders of magnitude smaller for VUV spectroscopy then for monochromatic VUV irradiation.

B. Electron cyclotron resonance (ECR) plasma

ECR plasma systems belong to the family of low-pressure, high electron-temperature discharges.[42] Here, the ECR system is used only to study the plasma-induced damage of dielectric wafers.

As shown in Figure 2, the ECR plasma system used here consists of a 2.45 GHz, 2 kW microwave generator, two

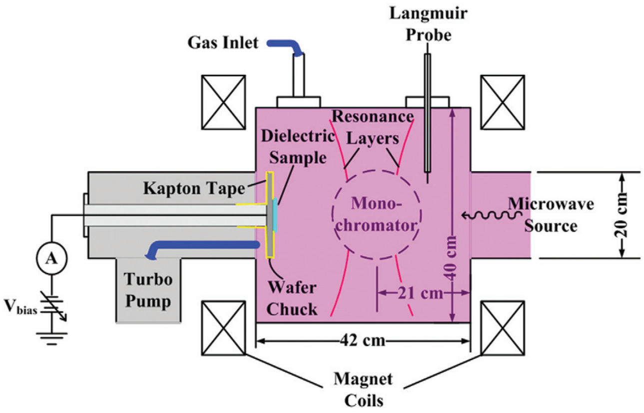

FIG. 2. Experimental setup for plasma exposure of dielectric films.

magnets arranged in a magnetic-mirror configuration, and a turbomolecular pump. Microwave radiation is coupled along the axis of the cylindrical vacuum chamber through an air-cooled quartz window. The turbomolecular pump is connected to the opposite end of the vacuum chamber. A mass-flow controller provides the gas feed.

For the cyclotron frequency of 2.45 GHz, electron cyclotron resonance occurs at a magnetic field of 875 G. The magnet current was adjusted to locate the cyclotron-resonant layer in the midplane of the vacuum chamber.

The use of magnetic fields in ECR discharges gives the user the ability to control the shape of the magnetic field and thus the shape of the plasma, which controls the uniformity across the wafer. For the operating conditions chosen in this work (20 mTorr pressure, He, 400 W microwave power), the spatially uniformity of the ECR system was assessed by exposing an unpatterned SiO_2/Si wafer to the ECR plasma and measuring the wafer surface potential using a Kelvin probe.[43] The measurement revealed little or no variation of the surface potential across the wafer. Hence, it was concluded that the ECR plasma is uniform across the wafer surface.

A monochromator was connected to the chamber to measure the VUV spectrum over a wavelength range from 50 to 300 nm. Ion density and electron temperature were monitored using a Langmuir probe. These parameters were used to calculate the photon spectrum emitted from the plasma.[6] In addition, a calibrated photodiode was used to measure the photon flux during plasma exposure. During plasma exposure, a capillary window over the sample was used when needed to separate charged-particle and VUV photon bombardment.[44]

IV. MEASUREMENT TECHNIQUES

A. Substrate/photoemission currents

Measurement of the photoemission and photoinjection currents can be used to calculate the number of trapped charges generated as a function of photon dose in the dielectric.[22,45] The difference between the photoemission/substrate current and the injection current as a function of photon dose is a measure of the number of trapped charges being created per unit time. The time integral of the trapped charges generated over the exposure time is the total number of trapped charges. Since the injection current is assumed constant, we can find the injection current from the steady-state photoemission/substrate current. This is graphically shown in Figure 3 and mathematically expressed as

$$Q(t) = \int_0^t [I_{pe}(\varphi) - I_{pi}(\varphi)]d\tau, \qquad (1)$$

where I_{pe} and I_{pi} are the photoemission and photoinjection currents as functions of photon dose φ. The photon dose is a monotonically increasing function of exposure time t. From Eq. (1), it is expected that if the photoinjection current is larger, the trapped charge accumulation will be lower.

B. VUV spectroscopy

From a device-performance perspective, it is very important to know the energy distribution, within the bandgap of SiOCH, of the trap states. For example, if the trap states line up in energy with electronic states within adjacent dielectrics or conductors, resonant-energy charge exchange can occur between the two material. Charge exchange with SiCOH and other materials can result in larger leakage currents and thus reduce the performance of microprocessors.

To determine the bandgap energy of SiCOH and the location of the trap states within the bandgap, we used VUV spectroscopic measurements on several low-*k* porous SiCOH dielectrics. VUV-spectroscopic measurements are made by measuring the substrate/photoemission currents as the photon energy is scanned. This results in peaks in the measured substrate/photoemission currents at various photon energies due to the excitation of electrons from specific electronic states to an energy above the conduction band of the dielectric layer. By comparing the photon energy at which the electronic states are excited with the energy levels calculated by first-principles studies[46] reported in the literature[47] the energy levels from which the electrons were excited can be determined.[48]

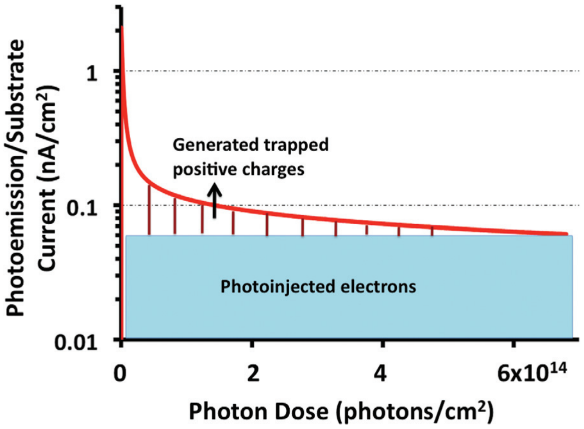

FIG. 3. Trapped charges from photoemission flux on a SiCOH sample as a function of dose of 8-eV VUV photons. Reprinted with permission from H. Sinha *et al.*, J. Vac. Sci. Technol. A **29**(3), 030602 (2011). Copyright © 2011 American Vacuum Society.

C. Surface-potential measurements

Surface-potential measurements,[49–54] obtained with a Kelvin probe, have been used for decades[55] as a technique for measuring charge induced on dielectric. Surface-potential measurements can give useful information about the net charge deposited on and within the dielectric layer such as trapped charge, mobile (free) charge, and surface charge.[56,57] As will be shown, the Kelvin probe can be of particular importance for the measurement of the trapped charge within dielectrics after VUV irradiation. In this section, the operation of the Kelvin-probe system and how it can be used to measure trapped charges within dielectric films is explained

A Kelvin probe is a noninvasive vibrating capacitor used to measure the surface potential of a charged dielectric on a conducting (or partially conducting) substrate.[58] Since the Kelvin probe is a noncontact device, the total charge on the dielectric can be measured without depleting/neutralizing any of the charge on the dielectric. A sketch of the Kelvin-probe system used here is shown in Figure 4. A capacitor is formed between the tip of the vibrating probe and the conductive substrate. The dielectric layer and an air gap are located between the electrodes of the capacitor. The measuring technique consists of vibrating (dithering) the probe above the dielectric surface, while simultaneously measuring the current through the capacitor as a function of time as the dc-bias voltage V_b is varied. An alternating current of the same frequency as the vibration frequency of the electrode will flow through the capacitor and is described by the following equation:

$$i = C_k \frac{dV}{dt} + V\frac{dC_k}{dt} = (V_{sp} + V_b)\frac{dC_k}{dt}, \qquad (2)$$

where C_k is the capacitance between the substrate and probe tip, V is the voltage across the capacitor, V_{SP} is the surface potential of the dielectric layer, V_b is the bias voltage in series with the substrate, and t is time. Note that the voltage across the vibrating capacitor is constant. Thus, the only current through the capacitor is due to the change in capacitance due to the motion of the vibrating probe. This current can be measured as a voltage drop across the resistor R shown in Figure 4. As can be seen from Eq. (2), when the bias voltage V_b is equal and opposite in polarity to the surface potential V_{SP}, the current through the vibrating capacitor is zero. This allows us to determine the surface potential on the dielectric underneath the probe tip. By scanning the probe tip across the surface of the dielectric, a two-dimensional surface-potential map can be obtained.

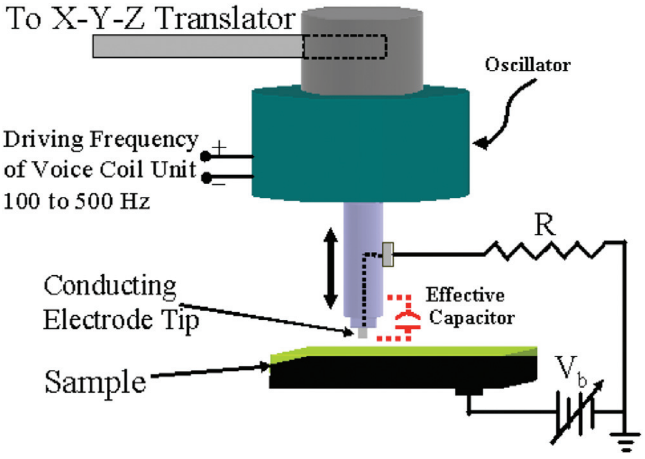

FIG. 4. Simplified circuit for the Kelvin probe system used to measure the surface potential of wafers after VUV exposure.

D. Capacitance-voltage characteristics

A mercury probe[59] is used to measure the capacitance vs. voltage (C-V) characteristics across Hg/dielectric/semiconductor structures. The C-V characteristics allow us to determine the amount of trapped charge within the dielectric films. The mercury drop is placed on the surface of the dielectric to form a metal/oxide/semiconductor (MOS) structure. The MOS structure is positioned on a probing station, housed in a light-tight box, and is connected by shielded cables to an inductance-capacitance-resistance (LCR) meter (Stanford Research Systems Model SR720). The LCR meter superimposes a small ac signal on top of a dc voltage that is stepped in increments of 1 V per minute. The ac signal is typically 15 mV rms or less at a frequency of 100 kHz. The LCR meter detects the resulting ac current flowing through the MOS structure and determines the capacitance as a function of voltage. For I-V characteristics, the steady-state current drawn through the dielectric is measured as a function of voltage with a Keithley 486 picoammeter.

The capacitance of the MOS structure varies as a function of the applied gate/metal voltage due to the accumulation or depletion of charge carriers (electrons, holes, or ion donors[60]) at the dielectric/semiconductor interface. Here we use the mercury probe to measure the MOS C-V characteristics in the "high-frequency" regime (>10 kHz).[43]

If there are charges located within the dielectric layer, then the entire C-V curve, including the flat-band voltage, will shift in proportion to the density and location of the charges within the dielectric. Assuming the charge distribution $\rho(x)$ varies in an arbitrary manner across the width of the dielectric layer the flat-band voltage shift can be expressed as[43]

$$\Delta V_{FB} = -\frac{1}{k\varepsilon_o}\int_0^d x\rho(x)dx, \qquad (3)$$

where x is the position with the dielectric layer measured from the Hg-dielectric interface and d is the thickness of the dielectric. Thus, the C-V characteristics obtained with the mercury probe are very useful and can be used to determine the amount of trapped charge within dielectric layer. In particular, by comparing the flat-band voltage before and after VUV and/or UV radiation we can evaluate the degree of charge accumulation within the dielectric layer due to radiation exposure.

E. Electron-spin resonance (ESR) spectroscopy

ESR is an extraordinary useful analytical tool[61] quite widely utilized for chemistry, biomedical, and solid-state physics research.[62] In particular, ESR can provide fairly detailed chemical and structural information about trapping centers within dielectrics and its interface with silicon provided that the trapping centers are paramagnetic.[45] This requirement of paramagnetism[63] is of great advantage for the relatively simple electrically active defect centers that are relevant to MOS device technology.[45] For example, most trapping centers within dielectrics or at the dielectric/Si interface will capture a single electron or a single hole. As a result, an initially diamagnetic center will be rendered paramagnetic (i.e., ESR "active") after trapping an electron or hole.[45] On the other hand, an initially paramagnetic center can be rendered diamagnetic (i.e., ESR "inactive") with the capture of either an electron or a hole.[45] In this way, ESR can identify the response of a defect center to charge carriers created during VUV irradiation, allowing us to identify the chemical and structural properties of defect center responsible for trapping charge.

In ESR spectroscopy, the sample under study is placed within a microwave cavity and then is exposed to a large slowly-varying magnetic field.[45] The microwave cavity is excited with a low-amplitude microwave signal typically in the microwave X band[64]: a microwave frequency $\nu > 9.5$ GHz.[45] For a fixed microwave frequency, paramagnetic defects within the sample will absorb the microwaves at specific magnetic fields since an unpaired electron has two possible orientations in the applied magnetic field and thus two possible energies.[45] Magnetic resonance occurs when the energy difference between the two electron orientations is equal to Planck's constant, h, times the microwave frequency.[45] For the very simple case of an isolated electron, the resonance requirement may be expressed as[45]

$$h\nu = g_o\beta_e B, \tag{4}$$

where the dimensionless factor $g_0 = 2.002319$, β_e (J/Tesla) is the Bohr magneton, h is Planck's constant, and B (Tesla) is the applied magnetic field.[45] Equation (7) describes the resonance condition for an electron that does not otherwise interact with its surroundings.[45] The structural information provided by ESR of a paramagnetic defect center within a solid is due to deviations from this simple expression.[45] For the relatively simple trapping centers studied in MOS systems, these deviations are due to spin-orbit coupling and electron–nuclear hyperfine interactions.[45] The spin-orbit coupling can be included in the ESR resonance condition by replacing the constant g_0 in Eq. (4) with the so called g-value[47] associated with the defect center under study. Thus, by monitoring the absorption of microwaves by the sample as the applied magnetic field is varied, the g-value of the paramagnetic center can be determined from the following expression:

$$g = \frac{h\nu}{\beta_e B}. \tag{5}$$

Quite a few defect centers within MOS defects have been identified with ESR. The most important defects are the E$'$ and P$_b$ centers.[45]

The ESR signals can be fitted, using the least-squares method, into Lorentzian derivatives which have the form of

$$f_{Lorentz}(B) = -\frac{\frac{2A(B-B_o)}{\sigma}}{\left[1+\left(\frac{B-B_o}{\sigma}\right)^2\right]^2}, \tag{6}$$

where A represents the amplitude of the signal, B_0 can be used to determine the g-factor of the defects, and σ is the width of the signal as the magnetic field is varied through resonance. The relative defect concentrations were calculated using the double integral of the signal as

$$C_{Lorentz} = \int\int_{B\,field} f'_{Lorentz}(B)dB\cdot dB = \pi A\sigma. \tag{7}$$

Absolute numbers of defects were obtained by comparison with a 0.0003% KCl weak-pitch sample (3.7×10^{13} spins/cm). The fingerprint of the defects, known as the g-factor, was calculated from the frequency and magnetic field strength as $g = 2.0033$. Using Eqs. (6) and (7), the changes to the defect concentrations in the dielectric were determined.[24,62,65]

V. DIELECTRIC MATERIALS

To investigate the effect of VUV, SiCOH samples of various dielectric constants and thicknesses were deposited on p-type silicon using plasma enhanced chemical vapor deposition (PECVD). The samples used here are shown in Table I. All three materials were produced with a single organosilane precursor. A structure forming and porogen molecule approach was not used. The deposition process took place in a capacitively coupled PECVD reactor with a radiofrequency source of 13.56 MHz in the presence of various inert and reactive gases as well as the above precursor. The process conditions such as pressure, RF power, precursor flow, and gas flows were varied to achieve desired film properties such as the dielectric constant, thickness, etc.

It is well known that plasma deposition induces defect states.[66] As a result, PECVD SiCOH dielectrics will likely exhibit non-ideal characteristics.

TABLE I. List of samples used for analysis of trapped charges generated in SiCOH.

	Dielectric layer	Dielectric constant	Thickness (nm)
		2.65	266
Charge trapping	SiCOH		444
		2.75	50[a]
Effect of UV curing	SiCOH	⋯	640[a]
			500
Effect of dielectric-substrate interface	SiCN/SiCOH/SiCN/Si SiCN/SiCOH/SiCN/oxide/Si SiCN/SiCOH/SiCN/Cu	SiCOH-2.4; SiCN-5	SiCOH-175; SiCN-15; Oxide-5
Effect of porosity	SiCOH	2.65	444
		3	458

[a] Pristine.

VI. SYNCHROTRON EXPOSURE

A. VUV spectroscopy

As mentioned earlier, VUV photons will cause depopulation of these defect states. VUV spectroscopy of a SICOH sample after irradiation with different photon doses can be used to show the depopulation effect as follows. Figure 5 shows four VUV-spectroscopic measurements between 5 and 15 eV taken after irradiating the dielectric with three different doses of 8-eV photons. Zero photon dose (no irradiation) is also shown for comparison. After the dielectric was irradiated with 8 eV photons, the peak due to defect states at 8 eV, as shown in Figure 5, reduces in magnitude relative to the other peaks at 6.2 and 9.6 eV. This result is consistent with findings of Yu *et al.*[67] and Atkin *et al.*[18] who claim the defect states in SiCOH to be located 0.15–0.3 eV below the conduction band and 0.5 eV above the valence band.[68,69] The height of the 8-eV peak is observed to increase as the 8-eV photon dose is increased. The magnitude of the peak at 8.0 eV eventually reaches a steady-state value for photon doses higher than 3×10^{13} photons/cm^2. We believe steady state is reached when all the defect states are depleted of electrons. That is, before VUV irradiation, the defect states are filled with electrons. During VUV irradiation, electrons are excited from the defect states to energies above the conduction band where they are photoemitted.

B. CV and surface potential measurements

We now compare the CV and surface-potential measurements after irradiation. A flat-band voltage of −2 V was observed for 266-nm SiCOH ($k = 2.65$). For a thicker sample, 444-nm SiCOH ($k = 2.65$) the flat-band voltage was −4 V. For VUV irradiation of 8 eV photons at a dose of 5.5×10^{14} photons/cm^2 incident on 266-nm thick SiCOH ($k = 2.65$), the flat-band voltage shifted to −4 V. This is shown in Figure 6 as V_{FB1}. The negative shift shows that the defect states have been depopulated of electrons by VUV irradiation resulting in more trapped positive charges. As photon dose increased, the flat-band voltage shifted more negatively until the flat-band voltage saturated at a maximum value of −6 V at a dose of 1.1×10^{15} photons/cm^2. This saturation flat-band voltage, V_{FB2}, is shown in Figure 6.

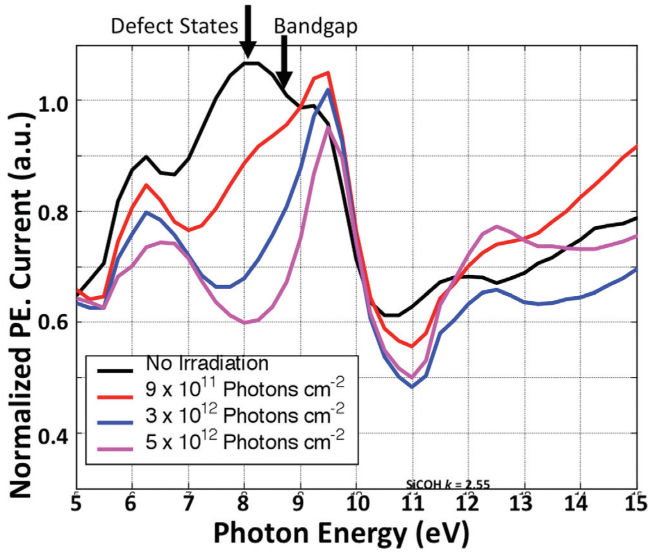

FIG. 5. VUV spectroscopic measurements on SiCOH after VUV irradiation of 8 eV VUV photons. Reprinted with permission from J. L. Lauer *et al.*, J. Electrochem. Soc. **157**(8), G177–G182 (2010). Copyright © 2010 The Electrochemical Society.

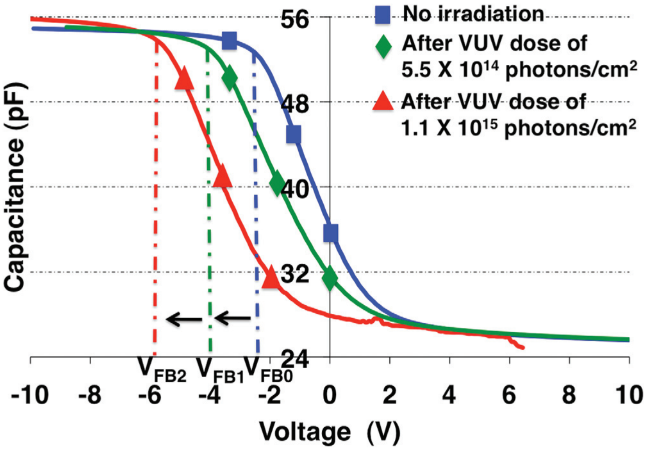

FIG. 6. Shifts in C-V characteristic for SiCOH ($k = 2.65$) with increasing VUV photon dose.

The surface potential also increased as the magnitude of the flat-band voltage increased. For the same photon dose (1.1×10^{15} photons/cm^2) that resulted in flat-band voltage saturation, the surface potential also saturated (Figure 7). This also implies that with increasing doses of VUV, more defect states were depleted of electrons. Thus, the maximum values of flat-band voltage and surface potential both occur when most of the defect states are depleted of electrons.

C. Effect of ultraviolet (UV) curing on charge trapping

In device fabrication, chemical-vapor deposited SiCOH glass is often cured with UV irradiation.[70–73] UV curing is

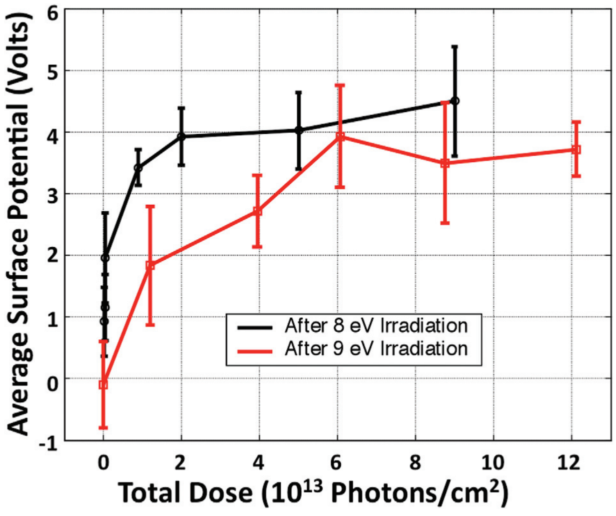

FIG. 7. Average surface potential as a function of total photon dose on SiCOH ($k = 2.55$) after irradiation with 8 and 9 eV VUV photons. Reprinted with permission from J. L. Lauer *et al.*, J. Electrochem. Soc., **157**(8), G177–G182 (2010). Copyright © 2010 The Electrochemical Society.

advantageous, yielding the benefits of improved hardness and corrosive strength of the dielectric.[74,75] However, by comparing the photoemission currents and surface-potential measurements for pristine SiCOH and UV-cured SiCOH, it is seen that more positively charged traps are generated in the UV-cured SiCOH compared to pristine SiCOH.[76] Furthermore, although UV curing reduces the number of defect states, we find that it can also increase both the intrinsic and photo-conductivities of SiCOH.

In steady state, the photoemission/substrate current can be used to find the defect density and photoconductivity of the dielectric. When the VUV photon energies are less than the bandgap energy, the following processes can occur[31,32,36,38]: (1) If the photon energy is greater than the energy difference between defect states in the bandgap and the vacuum, electrons trapped in these defect states can be directly photoemitted. (2) If the photon energy is less than the energy difference between the defect states in the bandgap and the vacuum, electrons can be excited into higher-energy defect states and then be photoemitted. (3) The VUV photons can excite electrons from the valence band into defect states, depending on the energy difference between the valence band and the defect states.

For processes (2) and (3), because the electrons travel through defect states before being photoemitted, the number of defect states is the controlling factor for the substrate/photoemission current. Hence, the greater the number of defect states, the larger the electron photoemission/substrate current for a given photon flux. Since the photon-flux density can vary with position, each incremental area of the dielectric generates a photoemission/substrate current density that is proportional to the photon flux over that incremental area. Hence, for photon energies less than the bandgap energy, the photoemission/substrate current in steady state is proportional to the defect-state density.

On the other hand, VUV photons with energies greater than the bandgap energy can be used to determine the sum of the intrinsic conductivity and the photoconductivity as follows. These photons can cause direct photoemission of electrons from *both* the defect states in the bandgap and the valence band since the density of states of electrons in the valence band is much greater than the defect-state density in the bandgap.[77] Hence, the electrons from the valence band will dominate the photoemission process.

The photoemitted electrons are collected and returned to the grounded substrate and then injected back into the dielectric. These electrons can travel to the vacant states in the valence band.[36] As these electrons flow back to the substrate, during steady state, the magnitude of the surface potential across the dielectric will depend on the parallel combination of the intrinsic and photo conductivities of the dielectric.[78,79] By finding the combined conductivity in this way and then finding the intrinsic conductivity as described below, the photoconductivity can be determined.

The intrinsic conductivity can be computed from the trapped-charge decay rate after VUV irradiation.[43,80] The trapped positive charges recombine with free electrons under influence of the self-consistent electric field.[38] In the absence of VUV photons, the drift motion of electrons under the influence of the self-consistent electric field in the dielectric is determined by the intrinsic conductivity. Since the surface potential is a measure of the amount of trapped charge in the dielectric, then from the decay rate of the surface potential the intrinsic conductivities and photoconductivities of both pristine and UV-cured SiCOH can be found and compared.[81]

To investigate these effects, 640 nm of low-*k* porous SiCOH dielectric was deposited on two Si wafers. One sample was kept pristine, while other sample was UV cured. After UV curing with a Novellus System SOLA®, the dielectric thickness was measured to be 500 nm using ellipsometry. The following measurements were made on pristine SiCOH and UV-cured SiCOH to compare charge trapping and conductivities. (1) Initial VUV spectroscopy, in which photoemission/substrate current is measured as a function of incident photon energy, between 4.5 and 12 eV. (2) 8 eV irradiation at a fixed energy but with much higher flux. The 8-eV photon dose was adjusted so as to achieve steady state. The photoemission/substrate current was measured as a function of time/dose during irradiation. (3) VUV spectroscopy was repeated after the 8-eV irradiation. (4) A set of surface-potential maps was generated with a Kelvin probe to observe the decay in surface potential as a function of time.

The number of trapped positive charges generated per unit area of 8 eV irradiation for pristine SiCOH and UV-cured SiCOH undergoing the same photon dose was compared. It was found that the UV-cured dielectric had approximately 5.6% more trapped positive charge in comparison to the pristine dielectric. Furthermore, it was also found that the photoinjection current in the UV-cured sample was approximately 7.9% less as compared with the pristine SiCOH sample. These results are shown in Table II. The measurements were found to be repeatable.

Then, by comparing the surface potential as a function of time after irradiation for both samples, we find that trapped charges in the UV-cured sample decay faster. The surface potential generated by VUV irradiation in the UV-cured sample decayed with a time constant of 0.116 V/h. In comparison, the surface potential decayed at 0.022 V/h for the pristine SiCOH. Thus, the charge-decay time constant for the UV-cured sample was five times that of the pristine sample. As discussed above, the UV-cured sample had only 5.6% more trapped charges after VUV irradiation. However the time taken for the trapped charges in the UV-cured SiCOH to decay was one third of that for pristine SiCOH. Thus, we can infer that the UV-cured dielectric films have a higher intrinsic conductivity. The intrinsic conductivity for pristine SiCOH, from the trapped charge decay rate, was calculated to be 1.43×10^{-16} S/m. As expected, the UV cured samples had a higher intrinsic conductivity of 7.57×10^{-16} S/m. These are summarized in Table III.

TABLE II. Comparison of trapped charges generated by 8-eV VUV photons, trapped charge decay time, and photoinjection flux for pristine and UV cured SiCOH.

	Pristine SiCOH 640 nm	UV cured SiCOH 500 nm
Trapped charges (#/cm^2)	8.03×10^{11}	8.48×10^{11}
Photoinjection current (pA/cm^2)	60.95	56.14
Trapped charges decay time (h)	75	23

Figure 8 shows the VUV spectroscopy curves for pristine and UV-cured SiCOH both before and after 8-eV VUV irradiation. Before VUV irradiation, the spectroscopy measurements for pristine and UV-cured SiCOH overlap. A small difference in the results is seen during VUV spectroscopy because an unavoidable small dose of VUV irradiation occurs while the spectroscopy scan was taken.

After VUV irradiation, VUV spectroscopy was made for comparison with the un-irradiated samples. The spectroscopy showed two important differences. First, for photon energies less than 8.5 eV as shown in Figure 8, the photoemission/substrate current measured during VUV spectroscopy for pristine SiCOH is larger than the corresponding current for UV-cured SiCOH. This occurs because, for photon energies less than 8.5 eV, photoemission can occur only from the defect states in the bandgap. Since the photoemission current will then be proportional to the number of defect states, we can conclude that pristine SiCOH has more defect states in the bandgap as compared to UV-cured SiOCH. On the other hand, for photon energies higher than 8.5 eV, the photoemission current for UV-cured SiCOH is larger than that for pristine SiCOH. This is because for energies greater than 8.5 eV, photoemission can occur directly from the valence band in addition to the photoemission from the defect states. In steady state, the photoemitted electrons are replaced with photoinjected electrons. These photoinjected electrons have to drift/diffuse to the surface of the dielectric to be photoemitted. Therefore, in steady state, the drift/diffusion current will be equal to the photoinjection current that in turn is equal to the photoemission/substrate current. Thus, as described above, the surface potential measured in steady state is determined by the parallel combination of the intrinsic and photoconductivities since the photoinjected current may be considered as a current source. Since the intrinsic conductivity has already been calculated, as described above, the photoconductivities for pristine and UV cured samples can easily be extracted from the surface potential and the steady-state current. As expected, the UV cured samples had a higher photoconductivity of 2.9×10^{-14} S/m in comparison to 2.0×10^{-14} S/m for pristine samples. These results are also summarized in Table III.

Hence, we can conclude that this sample of UV-cured SiCOH has fewer defect states than pristine SiCOH, especially if the comparison is made after VUV exposure. In addition, the UV-cured SiCOH has a higher photoconductivity. From calculations of the trapped charge, we find that UV-curing increases the number of trapped charges generated in SiCOH under VUV irradiation for the same photon dose and energy. However, it must be noted that all UV curing processes are not the same, and there are materials in which the leakage currents are smaller after UV curing.

TABLE III. The calculated intrinsic and photo conductivities of pristine and UV cured SiCOH.

	Pristine SiCOH	UV cured SiCOH
Intrinsic conductivity (S/m)	1.43×10^{-16}	7.57×10^{-16}
Photoconductivity (S/m)	2.0×10^{-14}	2.9×10^{-14}

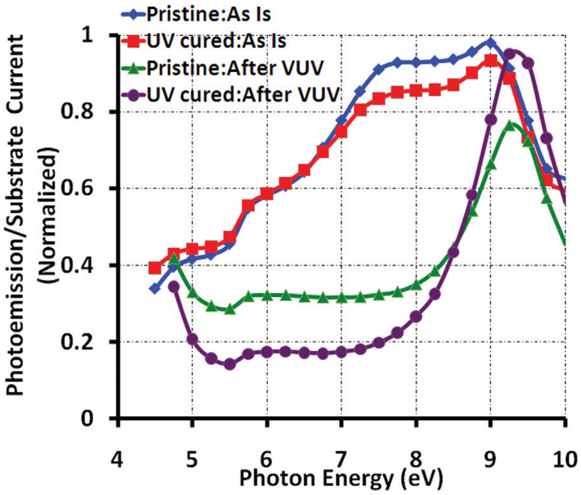

FIG. 8. VUV spectroscopy at 4.5–10 eV for pristine and UV cured SiCOH before and after 8-eV VUV irradiation. Reprinted with permission H. Sinha *et al.*, J. Vac. Sci. Technol. A **29**(3), 030602 (2011). Copyright © 2011 American Vacuum Society.

D. Effect of dielectric-substrate interface on charge trapping

In BEOL processing, a SiCOH/SiCN stack is typically deposited on an exposed Cu/SiCOH following CMP,[82] whereas the work reported in the previous section was for simple stacks of SiCOH/Si. The purpose here is to determine what differences in VUV response are observed for industrially relevant SiCN/SiCOH/SiCN/Cu stacks exposed to plasma etch, as compared to samples on Si with or without native oxide, similar to those described in other sections.[83–85] Here, dielectric films deposited on Cu and, for comparison, model Si/SiO2 films were irradiated with VUV photons having energies and fluxes typically generated during plasma processing. It was found that the nature of the dielectric-substrate interface changes the number of trapped charges in the dielectric.

To investigate the effect of different dielectric-substrate interfaces on charge trapping, a dielectric stack consisting of 15 nm SiCN($k=5$)/175 nm SiCOH($k=2.4$)/15 nm SiCN($k=5$) was deposited with plasma-enhanced chemical vapor deposition on the following substrates: (1) Si, (2) Si with 5-nm of thermally grown oxide, and (3) Cu/Ta/NiSi deposited on Si. SiCN forms an interface with these three substrates. A description of the samples is shown in Figure 9.

All of the samples have the same dielectric stack but have different dielectric-substrate interfaces. The dielectric stack deposited on silicon was used as a reference and compared with the other two. In comparison to the reference sample, the presence of a thin thermally grown oxide layer reduces the density of interface defect states.[86] This occurs because the dangling bonds from the silicon-crystal termination are reduced in the presence of the oxide.[87]

The reduced interfacial states result in a smaller Fowler-Nordheim tunneling current.[88,89] Fowler Nordheim tunneling is associated with electrons tunneling from the semiconductor Fermi level into the dielectric conduction band. Under

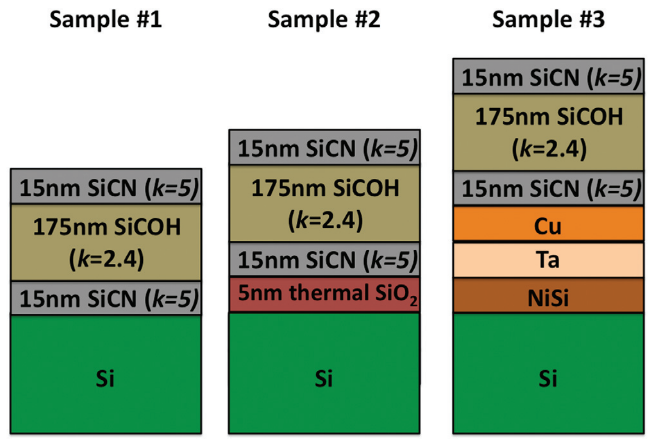

FIG. 9. A dielectric stack of SiCN/SiCOH/SiCN deposited on three different substrates.

Fowler-Nordheim conditions, it is possible for charge to tunnel from the valence band of the substrate into a trap/defect state in the bandgap of the dielectric. Thus, the number of interface states controls the tunneling current. Hence, the net injection current into the dielectric from the substrate will be smaller when there are fewer interface states. A lower injection current means less repopulation of the depopulated defect states, since, as stated previously, the steady-state condition is the result of a balance between depopulation by photon excitation and repopulation by injection. Hence, more positively charged traps remain in the sample deposited on Si with the interfacial thermal oxide as compared with the reference sample.

The following measurements were made during irradiation. First, VUV spectroscopy was performed for photon energies between 4.5–12 eV. Second, the sample was irradiatied with 8-eV VUV irradiation with a fluence of 5.9×10^{13} photons/cm^2. The photoemission/substrate current was measured as a function of time/dose during the irradiation. Finally, VUV spectroscopy was repeated after the 8-eV VUV irradiation.

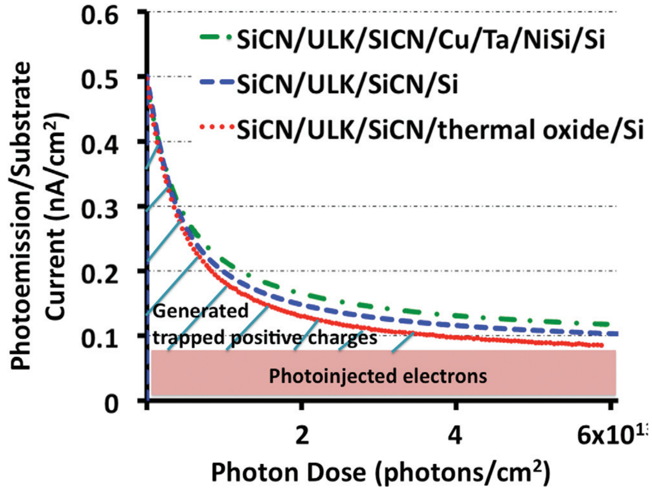

FIG. 10. Photoemission flux of SiCN/SiCOH/SiCN deposited on Cu, Si, and Si with thermal oxide as a function of increasing dose of 8-eV VUV photons. Reprinted with permission from H. Sinha *et al.*, Thin Solid Films, **519**(16), 5464–5466 (2011). Copyright © 2011 Elsevier.

Figure 10 shows the photoemission/substrate current measured during the 8-eV irradiation. As expected, the substrate current decreases with increasing photon dose for the three samples. The current is found to be same for all three samples at the lower doses. This is because the samples are fabricated with the same dielectric stack, and, hence, they are likely to generate the same number of photoemitted electrons from depopulation of the dielectric. This will occur until the dose increases so that the self-consistent electric field created by the trapped positive charges builds up to a sufficiently high level to change the photoemission/substrate currents.

In steady state, we see that the dielectric deposited on copper has the largest photoemission current, whereas the dielectric deposited on Si with the interfacial thermal oxide has the lowest steady-state photoemission current. This occurs because the SiCN-Cu interface has a lower energy barrier (0.9 eV) in comparison to SiCN-Si (1.7 eV).[90–92] On the other hand, the interface energy barrier between SiCN and Si with thermally grown oxide is higher than SiCN-Si because of reduced dangling bonds in the presence of the oxide.[87]

The number of trapped charges per unit area generated as a function of photon fluence per unit area can be calculated from the photoemission current measurements, as described previously. The calculated value of trapped charges for the three samples after a VUV photon dose of 5.9×10^{13} photons/cm^2 is shown in Table IV. The injection current, which is sum of the photoinjection and Fowler-Nordheim tunneling currents, is also listed in Table IV. From the tabulated data, the inverse relation between the number of trapped charges in the dielectric and the magnitude of the injection current is verified. The dielectric deposited on Si with an interfacial thermal oxide had the most trapped charges per unit area, followed by the dielectric stack on Si. The dielectric stack on Cu had the smallest number of trapped charges per unit area.

The results obtained from the substrate-current measurements were validated with VUV spectroscopy measurements between 4.5 and 12 eV. These are shown in Figure 11. We observe that the VUV spectroscopy curves for the three samples before irradiation are similar. These variations in the VUV spectroscopy curves are again likely the result of the low-level but unavoidable irradiation during VUV spectroscopy. The photon flux was made as small as possible. However after 8-eV VUV irradiation, the dielectric stack on Cu

TABLE IV. Comparison of trapped charges generated by 8-eV VUV photons and photoinjection flux for SiCN/SiCOH/SiCN deposited on Cu, Si, and Si with thermal oxide. The percentage increase or decrease in the trapped charge compared with the reference (top line) sample is indicated in the left-hand column.

	Trapped charges (#/cm^2)	Photoinjection current (pA/cm^2)
Stack/Si	2.25×10^{11}	103.4
Stack/oxide/Si	2.49×10^{11} (+10.7%)	84.6
Stack/Cu	2.00×10^{11} (−11.1%)	118.2

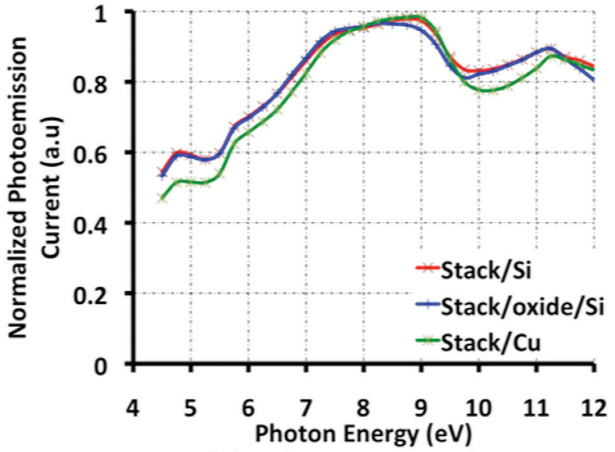

(a) Before VUV irradiation

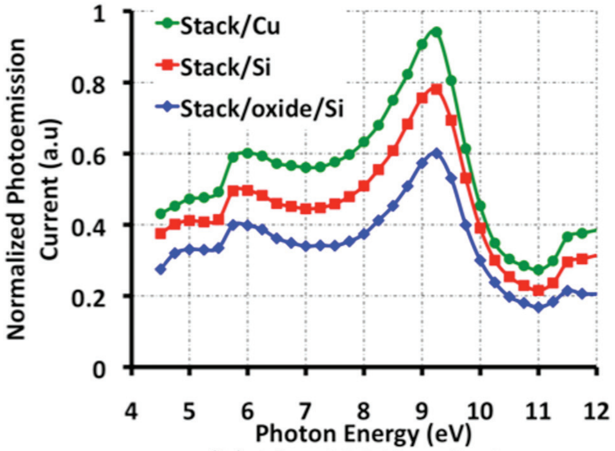

(b) After VUV irradiation

FIG. 11. VUV spectroscopy at 4.5–12 eV for SiCN/SiCOH/SiCN deposited on Cu, Si, and Si with thermal oxide (a) before VUV irradiation (b) after 8-eV VUV irradiation. Reprinted with permission from H. Sinha *et al.*, Thin Solid Films, **519**(16), 5464–5466 (2011). Copyright © 2011 Elsevier.

had the largest VUV spectroscopy current while the dielectric stack on Si with thermally grown interfacial oxide had the lowest VUV spectroscopy current. This result is true for any photon energy between 4.5 and 12 eV and is consistent with the substrate/photoemission measurements discussed earlier.

Thus, we find that the nature of the dielectric-substrate interface changes the number of trapped charges generated in the dielectric under VUV irradiation. As stated earlier, this is because a lower dielectric-substrate interface energy barrier increases the photoinjection current, thereby reducing the number of trapped charges generated in the dielectric. Inversely, a lower photoinjection current due to a higher dielectric-substrate interface barrier energy increases the number of trapped charges generated in the dielectric. Also the higher Fowler-Nordheim tunneling currents due to the increased number of interface defect states increases the injection current and reduces the number of trapped charges generated in the dielectric during VUV irradiation.

E. Effect of porosity on charge trapping

The dielectric constant of SiCOH can often be reduced by introducing porosity.[1,41,93,94] However, higher porosities show an increase in the number of trapped charges generated from incident VUV irradiation.[6,29] VUV spectroscopy, photoemission current, capacitance-voltage characteristics, and surface potential measurements are used to determine number of trapped charges generated for the three cases.

Typically, nanopores of size 2.5 nm or less are introduced in SiCOH to reduce the dielectric constant.[1,95] However, the nanopores can act as charge trapping centers.[31] That is, charges aggregate along the boundaries of pores and remain trapped. Thus, the number of trapped charges in SiCOH will change as the porosity increases.

The number of trapped charges generated per unit dose of VUV irradiation depends on the photoabsorption coefficient of the dielectric. The higher the photoabsorption coefficient, the more charges will be trapped. It has been reported that VUV photoabsorption increases with increasing porosity of SiCOH. Thus it is indeed plausible that for the same dose of VUV photons, higher porosity (lower dielectric constant) SiCOH will have more trapped charges in comparison to lower porosity (higher dielectric constant) SiCOH.

To investigate the effect of porosity on charge trapping, SiCOH with dielectric constants of 3.0 and 2.65 was deposited with thicknesses of 458 nm and 444 nm, respectively, on Si followed by UV curing. The porosity for $k = 2.65$ was measured to be 15%–20% by elipsometric porosimetry. The sample with $k = 3.0$ had no detectable porosity. After UV curing, surface-potential measurements and C-V measurements were made. The samples were then exposed to a fluence of 7×10^{13} photons/cm^2 of 8 eV VUV photons. The photoemission/substrate current was measured as a function of time/dose during irradiation. After VUV irradiation, the surface potential and C-V measurements were repeated.

Figure 12 shows the photoemission/substrate current of SiCOH for $k = 2.65$ and $k = 3.0$ as a function of the 8-eV VUV photon dose. Both measurements were made during the same synchrotron beam-current condition. The sample with $k = 2.65$ shows a higher photoemission/substrate current for the same VUV irradiation flux rate. This means that a higher percentage of photons was absorbed in the $k = 2.65$ dielectric film. This is validated by a VUV reflectance measurement[96] for the two samples, which is shown in Figure 13. The

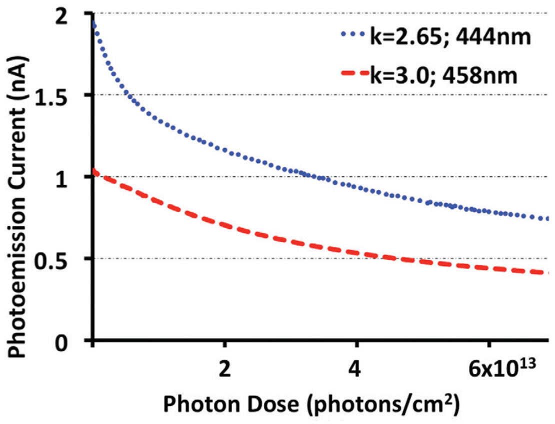

FIG. 12. Photoemission/substrate current of $k = 2.65$ 444 nm and $k = 3.0$ 458 nm SiCOH as a function of increasing 8-eV VUV photon dose.

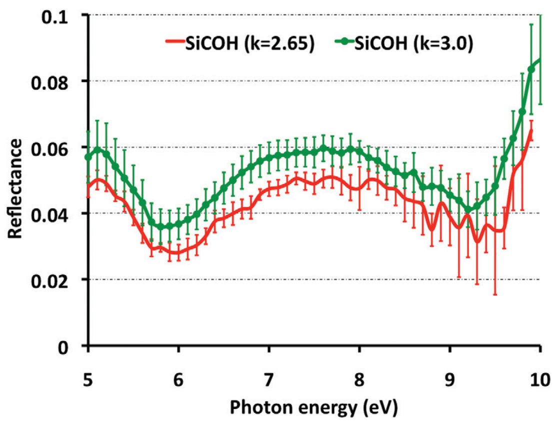

FIG. 13. Measured reflectance for $k = 2.65$ and $k = 3.0$ SiCOH for 5–10 eV photon energies. Reprinted with permission from H. Sinha *et al.*, J. Vac. Sci. Technol. A **28**(6), 1316–1318 (2010). Copyright © 2010 American Vacuum Society.

reflectance shows that the film with $k = 2.65$ has a lower reflectance, i.e., a higher photoabsorption.

The photoemission/substrate currents for the films with $k = 2.65$ and $k = 3.0$ as a function of photon dose can also be compared. With increasing VUV photon dose, more trapped charges are generated, which results in a higher self-consistent electric field. The self-consistent electric field reduces photoemission.[38] As shown in Figure 12, the slope of the photoemission/substrate current curve as photon dose increases changes rapidly for the film with $k = 2.65$ in comparison to the film with $k = 3.0$. This is likely because a larger self-consistent electric field builds up in the $k = 2.65$ dielectric in comparison to the $k = 3.0$ dielectric for the same VUV photon dose. Hence, we infer that more trapped charges are generated in the SiCOH with $k = 2.65$ for the same VUV photon dose.

The number of trapped charges generated from VUV irradiation is calculated from the photoemission/substrate current as was shown previously. For the $k = 2.65$ dielectric, a photon dose of 7×10^{13} photons/cm^2 generated 3.7×10^{11} trapped charges per square cm of the irradiated sample whereas for the $k = 3.0$ dielectric, only 2.3×10^{11} trapped charges per square cm were generated. This result can also be confirmed with surface-potential measurements. The surface potential increased by 5.4 V for the $k = 2.65$ dielectric, but increased only by 3.7 V for the $k = 3.0$ dielectric. This is consistent with the shift in the flat-band voltage of the C-V characteristics as was shown previously. A summary of these results is shown in Table V.

TABLE V. Trapped charges, surface potential and C-V characteristic flat-band voltage shift for $k = 2.65$ 444 nm and $k = 3.0$ 458 nm SiCOH after 8-eV VUV irradiation.

	k = 2.65, 444 nm	k = 3.0, 458 nm
Trapped charges (#/cm^2)	3.65 × 1011	2.29 × 1011
Surface potential (V)	5.4	3.7
C-V flat-band voltage shift (V)	(−) 5.9	(−) 4.2
Photoinjection current (pA)	0.739	0.41

Thus, it can be concluded that trapped charges in SiCOH due to VUV irradiation during processing are dependent on the porosity of the dielectric. More trapped charges are generated in higher porosity SiCOH for the same photon dose.

VII. PLASMA EXPOSURE

A. Charge accumulation in low-k dielectrics

Here we investigate how charges can be generated in the dielectric stacks during plasma exposure as well as how they leak away after exposure. That is, we now expose the samples to simultaneous VUV/UV and particle bombardment. Hence, low-*k* porous organosilicate glass (SiCOH) was exposed to an argon ECR plasma. The ECR plasma was operated with a pressure of 5 mTorr and a microwave power of 400 W. *In situ* substrate currents at the wafer chuck and VUV photon-flux measurements with a monochromator were measured followed by surface-potential measurements on the dielectric before and after exposure.

Two different charging mechanisms occur during argon plasma exposure. They are (1) ion sticking and (2) photon bombardment. The ion density was measured with a Langmuir probe, including the sheath effects, while the photon flux was measured with the VUV monochromator. The plasma potential was also measured using the Langmuir probe. We calculate the ion flux by assuming that ions enter the sheath with the Bohm velocity. The wafer chuck is normal to the magnetic field lines, so that a high ion flux is incident on the dielectric. The magnetic field, plasma neutral pressure, microwave power, wafer-bias voltage, and wafer position can all be adjusted to control the fluxes of the charged particles and photons. Figure 14 shows the measured spatial distribution of the ion density in the plasma chamber (a) along with the measured argon ECR plasma radiation spectrum in the VUV range (b). The photon flux was measured using a monochromator that was connected to the plasma chamber. The absolute flux was obtained using a calibrated photodiode.

As mentioned previously, a capillary-array window was placed over a portion of the dielectric. The window filters out the ion flux while allowing photons to travel to the dielectric, so that ion and photon bombardment effects on dielectric charging can be separated.

The charge accumulation after plasma exposure was measured, as shown in Figure 15. Immediately after plasma exposure, the samples with and without the capillary-array window exhibit different surface potentials (8.5 and 15.3 V, respectively). In addition, the time-decay rates of the surface-potential of the samples after exposure are different as shown in Figure 15. The surface potential of the sample that is not covered by the window shows a faster initial decay. When it reaches the surface-potential curves for the samples with synchrotron exposure and for plasma exposure with the capillary-array window about one hour after plasma exposure, it follows them exactly.

This shows that ion and photon bombardment accumulate charge in the dielectric with different mechanisms. For ion bombardment, more charge was accumulated, but it decays faster in time after exposure. This is likely due to

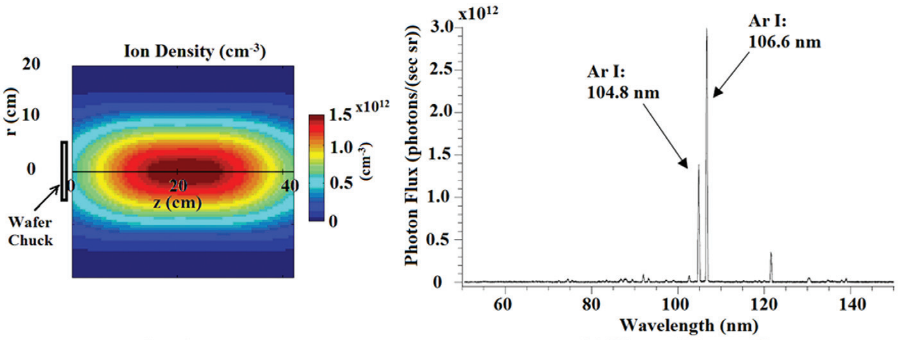

(a) Ion density (b) Plasma Photon Flux

FIG. 14. Plasma diagnostics for (a) ion density and (b) photon flux from ECR plasma.

surface ion sticking. On the other hand, photon bombardment is likely to result in trapped charge within the dielectric layer with a much longer decay time. The decay for these trapped charges is likely from the leakage current through the dielectric layer. This interesting phenomenon leads to the conclusion that there are indeed different mechanisms of charge accumulation from particle bombardment and from radiation bombardment.

To confirm this, a separate 11.6 eV VUV synchrotron irradiation was made on SiCOH. In Figure 15, it is seen that the surface-potential decay rate after synchrotron or plasma radiation exposure (the case with the capillary-array window) are roughly the same. Hence, we conclude that the charge-accumulation mechanism of the window-covered sample is due to photon bombardment and is not affected by the small number of particles that might have been able to pass through the capillary-array window. For the sample that is not covered by the window, the rapid decay of the surface potential is likely due to contact with the air of the ions implanted on the surface. In fact, keeping the sample under vacuum until the surface potential was actually measured was shown to greatly delay the initial charge-neutralization process.

B. Modifications of chemical bonds and physical changes

It has been reported by Lee and Graves[97] that 8.4 eV VUV irradiation can result in broken Si–C bonds. Thus, after VUV irradiation this material would be expected to have a larger number of Si dangling bonds. By using the plasma exposure system and the capillary-array window, it is possible to examine the response to VUV irradiation from plasma exposure without the presence of ion bombardment. ESR measurements on pristine (SiCOH with $k = 2.75$ and 50 nm thickness) and plasma-exposed samples with and without the capillary-array window are shown in Figure 16. By fitting the ESR measurement curve using A, B_0, and σ to determine the defect concentration (Table VI), it is seen that the defect concentration increases due to VUV irradiation. The defect concentration increases further if no capillary array window was used during plasma-exposure, i.e., ion bombardment is added to the VUV photon irradiation.

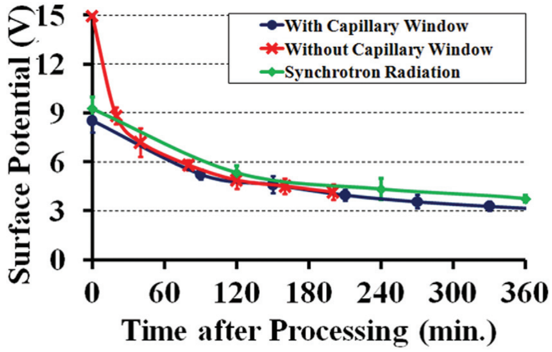

FIG. 15. Surface potential time decay of 231 nm SiCOH after plasma exposure.

In addition to ESR measurements, changes in chemical properties were measured using Fourier transform infrared spectroscopy (FTIR). Multiple chemical bonds were identified: Si-$(CH_3)_{x=1,2,\text{or}3}$ at 700–900 cm^{-1}, Si-O stretch band at 970–1250 cm^{-1}, Si-CH_3 at 1274 cm^{-1}, C=O at 1710 cm^{-1}, Si-H at 2220 cm^{-1}, and CH_x at 2970 cm^{-1}.[1,44] Figure 17 shows FTIR measurements of the pristine and plasma-exposed SiCOH with and without the capillary-array window. From Figure 17, we see that the FTIR shows the Si-$(CH_3)_x$ wagging concentrations increase due to plasma-photon bombardment. The concentration is even higher for the uncovered sample, suggesting that plasma exposure also

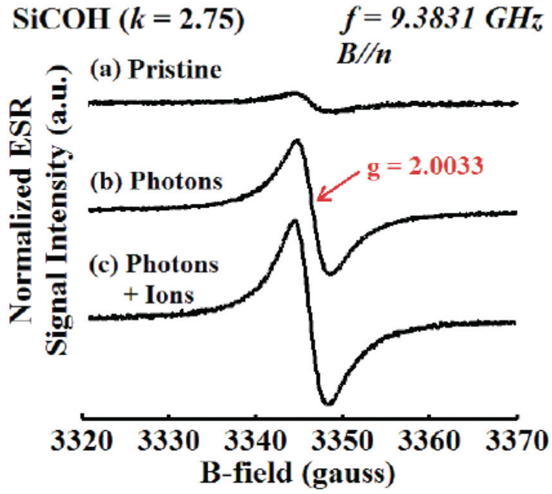

FIG. 16. ESR signals for (a) pristine SiCOH (b) after plasma exposure with capillary-array window, and (c) after plasma exposure without capillary-array window.

TABLE VI. Fitting parameters of ESR signal and calculated defect concentrations for measurements on pristine and with and without capillary-array window plasma exposed SiCOH.

	[B0, A, σ] (gauss, 1, gauss)	Photoinjection current (pA/cm^2)
Pristine	3346.32, 0.043, 4.02	1.17 × 1013
VUV irradiation	3346.17, 0.321, 3.93	8.54 × 1013
Ion bombardment and VUV irradiation	3346.16, 0.413, 3.93	1.10 × 1014

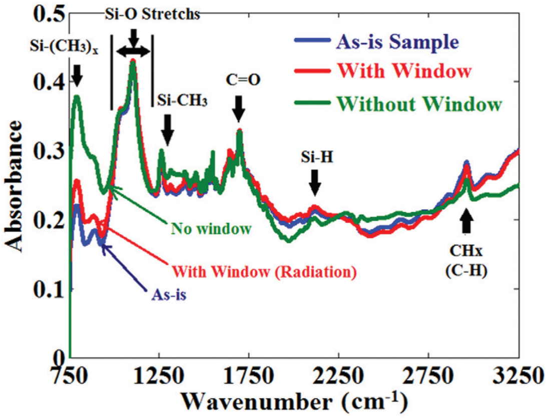

FIG. 17. Fourier transform infrared measurements of pristine and with and without capillary-array window plasma exposed SiCOH.

increases the Si-$(CH_3)_x$ wagging concentration by ion bombardment. Note that the increase of Si-$(CH_3)_x$ wagging does not indicate any chemical reaction taking place. It only indicates that, the dielectric film was subject to a physical change so that a more twisted bonding structure was seen during the processing.

VIII. SUMMARY AND CONCLUSIONS

VUV damage effects on low-*k* dielectric films were identified with both synchrotron and plasma exposure. Photons from the plasma cause trapped-charge accumulation in the bulk of the dielectric, while ions tend to stick to the dielectric surface. Chemical-bonding structures were identified along with physical changes to the low-*k* dielectrics due to plasma and VUV exposure. By analyzing measurements of photoemission currents and VUV spectroscopy, C-V characteristics and surface potential measurements, it was found that VUV irradiation depopulates electrons in the defect states leaving the trapped positive charges in the dielectric. The number of positively charged traps generated by VUV irradiation during processing is altered by the material properties of SiCOH. More trapped charges per unit photon dose are generated in UV-cured SiOCH than in pristine SiCOH during VUV irradiation. Although there are major advantages to UV curing of low-*k* dielectrics, there are thus some deleterious effects on its intrinsic and photo conductivities as well as enhanced charge trapping that are of importance in plasma processing of low-*k* SiCOH. In addition, changing the dielectric-substrate interface can change the number of positively charged traps generated in the dielectric during processing. Higher porosity in SiCOH has the advantage of a lower dielectric constant, but has the disadvantage of more positively charged traps being generated during VUV irradiation. It is likely that the increase in trapped charge is ascribed to higher photoabsorption and charge trapping around the nanopores. Consequently, modifications of the porosity, the dielectric-substrate interface and the UV curing process can be used as parameters to reduce positive charge accumulation during processing of low-*k* SiCOH.

Using a capillary-array window, it is now possible to separate particle-bombardment and plasma-radiation effects during ECR plasma exposure on SiCOH. It was found that plasma-induced charge accumulation has two parts: (1) surface ion sticking from ion bombardment and (2) trapped-charge accumulation within the dielectric due to photon bombardment. ESR measurements showed an increase in defect state concentration and FTIR measurement showed modification Si–$(CH_3)_x$ bond concentrations with plasma exposure.

The authors hope that the results presented in this review paper will be helpful in developing the future applications of low-k dielectric materials.

ACKNOWLEDGMENTS

The authors would like to acknowledge several helpful conversations with A. Grill. This work has been supported by the Semiconductor Research Corporation under Contact No. 2008-KJ-1871 and by the National Science Foundation under Grant CBET-1066231. The UW-Madison Synchrotron is funded by NSF under Grant DMR-0537588.

[1] A. Grill, J. Appl. Phys. **93**, 1785 (2003).
[2] W. Volksen, R. D. Miller, and G. Dubois, Chem. Rev. **110**, 56–110 (2010).
[3] E. T. Ogawa, J. Kim, G. S. Haase, H. C. Mogul, and J. W. McPherson, in Proceedings of IEEE International Reliability Physics Symposium, IEEE, Dallas, TX, 2003, p. 166.
[4] K.-Y. Yiang, H. W. Yao, A. Marathe, and O. Aubel, in Proceedings of 44th Annual IEEE International Reliability Physics Symposium, IEEE, Montreal, QC, 2009.
[5] F. Chen, O. Bravo, K. Chanda, P. McLaughlin, T. Sullivan, J. Gill, J. Lloyd, R. Kontra, and J. Aitken, in Proceedings of 44th Annual IEEE International Reliability Physics Symposium, IEEE, New York, 2006.
[6] C. Guedj, E. Martinez, and G. Imbert, Charging and Aging Effects in Porous ULK Dielectrics (Mater. Res. Soc. Symp. Proc., 2007), Vol. 990.
[7] M. T. Nichols, H. Sinha, C. A. Wiltbank, G. A. Antonelli, Y. Nishi, and J. L. Shohet, Appl. Phys. Lett. **100**, 112905 (2012).
[8] C. Cismaru and J. L. Shohet, Appl. Phys. Lett. **74**, 2599–2601 (1999).
[9] J. R. Woodworth, M. G. Blain, R. L. Jarecki, T. W. Hamilton, and B. P. Aragon, J. Vac. Sci. Technol. A **17**, 3209–3217 (1999).
[10] J. R. Woodworth, M. E. Riley, V. A. Amatucci, T. W. Hamilton, and B. P. Aragon, J. Vac. Sci. Technol. A **19**, 45–55 (2001).
[11] S. Uchida, S. Takashima, M. Hori, M. Fukasawa, K. Ohshima, K. Nagahata, and T. Tatsumi, J. Appl. Phys. **103**, 073303 (2008).
[12] M. Joshi, J. P. McVittie, and K. Saraswat, in 7th International Symposium on Plasma- and Process-Induced Damage, Maui, HI, 2002, p. 23.
[13] J. L. Lauer, J. L. Shohet, C. Cismaru, R. W. Hansen, M. Y. Foo, and T. J. Henn, J. Appl. Phys. **91**, 1242 (2002).
[14] J. L. Lauer, J. L. Shohet, and Y. Nishi, Appl. Phys. Lett. **94**, 162907 (2009).
[15] G. S. Upadhyaya, J. L. Shohet, and J. B. Kruger, Appl. Phys. Lett. **91** 182108 (2007).
[16] C. Cismaru, J. L. Shohet, J. L. Lauer, R. W. Hansen, and S. Ostapenko, Appl. Phys. Lett. **77**, 3914 (2000).
[17] J. L. Lauer, G. S. Upadhyaya, H. Sinha, J. B. Kruger, Y. Nishi, and J. L. Shohet, J. Vac. Sci. Technol. A **30**, 01A109 (2012).
[18] J. M. Atkin, E. Cartier, T. M. Shaw, R. B. Laibowitz, and T. F. Heinz, Appl. Phys. Lett. **93**, 122902 (2008).

[19] J. R. Lloyd, E. Liniger, and T. M. Shaw, J. Appl. Phys. **98**, 084109 (2005).

[20] J. M. Atkin, D. Song, T. M. Shaw, E. Cartier, R. B. Laibowitz, and T. F. Heinz, J. Appl. Phys. **103**, 094104 (2008).

[21] G. B. Alers, K. Jow, R. Shaviv, G. Kooi, and G. W. Ray, IEEE Trans. Device Mater. Reliab. **4**, 148 (2004).

[22] H. Ren, H. Sinha, A. Sehgal, M. T. Nichols, G. A. Antonelli, Y. Nishi, and J. L. Shohet, Appl. Phys. Lett. **97**, 072901 (2010).

[23] G. S. Upadhyaya, "Effects of vacuum-ultraviolet radiation on the plasma-induced charging of patterned-dielectric materials" Ph.D. dissertation (University of Wisconsin-Madison, Madison, WI, 2008).

[24] J. D. Chatterton, G. S. Upadhyaya, J. L. Shohet, J. L. Lauer, R. D. Bathke, and K. Kukkady, J. Appl. Phys. **100**, 043306 (2006).

[25] Y. Li, G. Groeseneken, K. Maex, and Z. Tokei, IEEE Trans. Device Mater. Reliab. **7**, 252 (2007).

[26] Y. Ichihashi, Y. Ishikawa, R. Shimizu, and S. Samukawa, J. Vac. Sci. Technol. B **28**, 829 (2010).

[27] Y. Ishikawa, Y. Katoh, M. Okigawa, and S. Samukawa, J. Vac. Sci. Technol. A **23**, 6 (2005).

[28] Y. Chao and N. Zhao-Yuan, Chin. Phys. B **19**, 057701 (2010).

[29] J. Planelles and J. L. Movilla, Phys. Rev. B **73**, 235350 (2006).

[30] J. Cazaux, J. Microscopy **188**, 106 (1997).

[31] H. Sinha, J. L. Lauer, M. T. Nichols, G. A. Antonelli, Y. Nishi, and J. L. Shohet, Appl. Phys. Lett. **96**, 052901 (2010).

[32] H. Sinha, M. T. Nichols, A. Sehgal, M. Tomoyasu, N. M. Russell, G. A. Antonelli, Y. Nishi, and J. L. Shohet, J. Vac. Sci. Technol. A **29**, 010601 (2011).

[33] Y. Ou, P.-I. Wang, M. He, T.-M. Lu, P. Leung, and T. A. Spooner, J. Electrochem. Soc. **155**, G283 (2008).

[34] R. J. Powell, J. Appl. Phys. **46**, 4557 (1975).

[35] R. S. Muller and T. I. Kamins, *Device Electronics for Integrated Circuits* (John Wiley & Sons, New York, 2003).

[36] J. L. Lauer, "The effect of vacuum ultraviolet irradiation on dielectric materials," Ph.D. dissertation (University of Wisconsin-Madison, Madison, WI, 2010).

[37] G. S. Upadhyaya, J. L. Shohet, and J. L. Lauer, Appl. Phys. Lett. **86**, 102101 (2005).

[38] H. Sinha, H. Ren, A. Sehgal, G. A. Antonelli, Y. Nishi, and J. L. Shohet, Appl. Phys. Lett. **96**, 142903 (2010).

[39] H. Sinha, J. L. Lauer, Y. Nishi, and J. L. Shohet, *Modeling the Effects of Vacuum-Ultraviolet Radiation during Processing Incident on Dielectric Materials that Include Defects* (American Vacuum Society, San Jose, 2009).

[40] H. Sinha and J. L. Shohet, J. Vac. Sci, Techonol. A **30**, 031505 (2012).

[41] H. Ren, "Plasma-processing-induced damage of thin dielctric films," Ph.D. dissertation (University of Wisconsin-Madison, Madison, WI, 2011).

[42] C. Cismaru, "Charging and vacuum-ultraviolet radiation effects on the plasma processing induced damage of semiconductor devices," Ph.D. dissertation (University of Wisconsin-Madison, Madison, WI, 1999).

[43] J. L. Lauer and J. L. Shohet, IEEE Trans. Plasma Sci. **33**, 248–249 (2005).

[44] M. Darnon, T. Chevolleau, T. David, N. Posseme, J. Ducote, C. Licitra, L. Vallier, O. Joubert, and J. Torres, J. Vac. Sci. Techonol. B **26**, 1964 (2008).

[45] C. Cismaru and J. L. Shohet, J. Appl. Phys. **88**, 1742 (2000).

[46] J. X. Zheng, G. Ceder, T. Maxisch, W. K. Chim, and W. K. Choi, Phys. Rev. **75**, 104112 (2007).

[47] E. P. O'Reilly and J. Robertson, "Theory of defects in vitreous silicon dioxide," Phys. Rev. B **27**, 3780 (1983).

[48] M. Benoit, M. Pohlmann, and W. Kob, Europhys. Lett. **82**, 57004 (2008).

[49] K. D. Cummings and M. Kiersh, "Charging effects from electron beam lithography," J. Vac. Sci. Technol. B **7**, 1536 (1989).

[50] H. Itoh, K. Nakamura, and H. Hayakawa, J. Vac. Sci. Technol. B **7**, 1532 (1989).

[51] M.-Y. Lee, J. R. Hu, W. Catabay, P. Schoenborn, and A. Butkus, "Comparison of CHARM-2 and surface potential measurement to montitor plasma induced gate oxide damage," in International Symposium on Plasma- and Process Induced Damage, Monterey, CA, 1999, p. 112.

[52] A. R. Frederickson and J. R. Dennison, IEEE Trans. Nucl. Sci. **50**, 2284 (2003).

[53] S. T. Lai, IEEE Trans. Plasma Sci. **31**, 1118 (2003).

[54] D. K. Scroder, Mater. Sci. Eng. **B91-91**, 196 (2002).

[55] A. Hoff, K. Nauka, T. Person, J. Lagowski, L. Jastrzebski, and P. Edelman, "A novel approach to monitoring of plasma processing equipment and plasma damage without test structures," Proc. IEEE/SEMI Adv. Semi. Man. Conf. (1997), p. 185.

[56] I. D. Baikie and P. J. Estrup, Rev. Sci. Instrum. **69**, 3902–3907 (1998).

[57] H. Sinha, J. L. Lauer, G. A. Antonelli, Y. Nishi, and J. L. Shohet, Thin Solid Films **520**, 5300 (2012).

[58] R. F. Pierret, *Semiconductor Device Fundamentals* (Addison-Wesley Publishing Company, 1996).

[59] D. D. Burkey and K. K. Gleason, J. Electrochem. Soc. **151**, F105 (2004).

[60] J. T. Ryan, P. M. Lenahan, G. Bersuker, and P. Lysaght, Appl. Phys. Lett. **90**, 173513 (2007).

[61] P. M. Lenahan and J. F. Conley, J. Vac. Sci. Technol. B **16**, 2134 (1998).

[62] A. Stesmans and V. V. Afanas'ev, Appl. Phys. Lett. **85**, 3792 (2004).

[63] P. T. Chen, B. B. Triplett, J. J. Chambers, L. Colombo, P. C. McIntyre, and Y. Nishi, J. Appl. Phys. **104**, 014106 (2008).

[64] H. Ren, S. L. Cheng, Y. Nishi, and J. L. Shohet, Appl. Phys. Lett. **96**, 192902 (2010).

[65] G. J. Park, T. Hayakawa, and M. Nogami, J. Phys.: Condens. Matter **15**, 1259 (2003).

[66] V. Ligatchev, T. K. S. Wong, B. Liu, and J. Rusli, Appl. Phys. Berlin **92**, 4605 (2002).

[67] S. Yu, T. K. S. Wong, K. Pita, X. Hu, and V. Ligatchev, J. Appl. Phys. **92**, 3338 (2002).

[68] J. L. Lauer, H. Sinha, M. T. Nichols, G. A. Antonelli, Y. Nishi, and J. L. Shohet, J. Electrochem. Soc. **157**(8), G177–G182 (2010).

[69] A. Grill, Annu. Rev. Mater. Res. **39**, 49 (2009).

[70] I. L. Berry, C. Waldfried, and K. Durr, Requirements and Constraints on Optimizing UV Processing of Low-k Dielectrics (Mater. Res. Soc. Symp. Proc., 2007), Vol. 990.

[71] V. Jousseaume, A. Zenasni, L. Favennec, G. Gerbaud, M. Bardet, J. P. Simon, and A. Humbert, J. Electrochem. Soc. **154**, G103 (2007).

[72] B. C. Bittel, P. M. Lenahan, and S. W. King, Appl. Phys. Lett. **97**, 063506 (2010).

[73] S. I. Nakao, J. Ushio, T. Ohno, T. Hamada, Y. Kamigaki, M. Kato, K. Yoneda, S. Kondo, and N. Kobayashi, in Proceedings of the IEEE International Interconnect Technology Conference, Burlingame, pp. 66–68, 2006.

[74] S. Eslava, F. Iacopi, A. M. Urbanowicz, C. E. A. Kirschhock, K. Maex, J. A. Martens, and M. R. Baklanov, J. Electrochem. Soc. **155**, G231 (2008).

[75] R. F. Pierret, *Semiconductor Device Fundamentals* (Addison-Wesley, Reading, MA, 1996).

[76] H. Sinha, G. A. Antonelli, Y. Nishi, and J. L. Shohet, J. Vac. Sci. Technol. A **29**, 030602 (2011).

[77] L. Mosquera, I. de Oliveira, J. Frejlich, A. C. Hernandes, S. Lanfredi, and J. F. Carvalho, J. Appl. Phys. **90**, 2635 (2001).

[78] M. Hosoya, K. Ichimura, Z. H. Wang, G. Dresselhaus, and P. C. Eklund, Phys. Rev. B **49**, 4981 (1994).

[79] H. J. Queisser and D. E. Theodorou, Phys. Rev. B **33**, 4027–4033 (1986).

[80] H. J. Queisser, Phys. Rev. Lett. **54**, 234–236 (1985).

[81] A. Grill, D. Edelstein, M. Lane, V. Patel, S. Gates, D. Restaino, and S. Molis, J. Appl. Phys. **103**, 054104 (2008).

[82] V. C. Ngwan, C. Zhu, and A. Krishnamoorthy, Appl. Phys. Lett. **84**, 2316 (2004).

[83] M. Fayolle, G. Passemard, O. Louveau, F. Fusalba, and J. Cluzel, Microelectr. Eng. **70**, 2–4 (2003).

[84] J. H. Stathis, D. A. Buchanan, D. L. Quinlan, A. H. Parsons, and D. E. Kotecki, Appl. Phys. Lett. **62**, 2682 (1993).

[85] H. Sinha, A. Sehgal, H. Ren, M. T. Nichols, M. Tomoyasu, N. M. Russell, Y. Nishi, and J. L. Shohet, Thin Solid Films **519**(16), 5464–5466 (2011).

[86] A. Stesmans and V. V. Afanas'ev, Appl. Phys. Lett. **82**, 4074 (2003).

[87] L. L. Chapelon, E. Petitprez, P. Brun, A. Farcy, and J. Torres, Microelectr. Eng. **84**, 11 (2007).

[88] M. Lenslinger and E. H. Snow, J. Appl. Phys. **40**, 278 (1969).

[89] C. Chen, W. L. Wilson, and M. Smayling, J. Appl. Phys. **83**, 3898 (1998).

[90] C. S. Chang, S. Chattopadhyay, L. C. Chen, K. H. Chen, C. W. Chen, Y. F. Chen, R. Collazo, and Z. Sitar, Phys. Rev. B **68**, 125322 (2003).

[91] Y. Lan, M. Yan, W. Liu, Y. Hu, and T. Lin, J. Vac. Sci. Technol. B **24**, 918 (2006).

[92] J.-M. Park and S.-W. Rhee, J. Electrochem. Soc. **149**, F92 (2002).

[93] C. L. Wang, M. H. Weber, and K. G. Lynn, J. Appl. Phys. **99**, 113514 (2006).

[94] L. Shen and K. Zeng, Microelectron. Eng. **71**, 221 (2004).

[95] M. R. Baklanov, K. P. Mogilnikov, V. G. Polovinkin, and F. N. Dultsev, J. Vac. Sci. Technol. B **18**, 1385 (2000).

[96] H. Sinha, D. B. Straight, J. L. Lauer, N. C. Fuller, S. U. Engelmann, Y. Zhang, G. A. Antonelli, Y. Nishi, and J. L. Shohet, J. Vac. Sci. Technol. A **28**, 1316 (2010).

[97] J. Lee and D. B. Graves, J. Phys. D: Appl. Phys. **43**, 425201 (2010).